Wang *et al. Chem. Synth.* **2025**, *5*, 34
DOI: 10.20517/cs.2024.159

Chemical Synthesis

Research Article

Open Access

Check for updates

Achieving photocatalytic water reduction and oxidation over narrow bandgap $FeVO_4$

Shuo Wang[1,#], Chunjiang Liu[1,#], Can Li[1], Ningning Wang[1], Chen-Yang Li[1], Zhongxu Yuan[1], Shanshan Chen[1,*], Fuxiang Zhang[2,*]

[1]School of Materials Science and Engineering, Nankai University, Tianjin 300350, China.
[2]State Key Laboratory of Catalysis, Dalian Institute of Chemical Physics, Chinese Academy of Sciences, Dalian 116023, Liaoning, China.
[#]Authors contributed equally.

[*]**Correspondence to:** Prof. Fuxiang Zhang, State Key Laboratory of Catalysis, Dalian Institute of Chemical Physics, Chinese Academy of Sciences, No. 457 Zhongshan Road, Shahekou District, Dalian 116023, Liaoning, China. E-mail: fxzhang@dicp.ac.cn; Prof. Shanshan Chen, School of Materials Science and Engineering, Nankai University, No. 38 Tongyan Road, Jinnan District, Tianjin 300350, China. E-mail: sschen@nankai.edu.cn

How to cite this article: Wang, S.; Liu, C.; Li, C.; Wang, N.; Li, C. Y.; Yuan, Z.; Chen, S.; Zhang, F. Achieving photocatalytic water reduction and oxidation over narrow bandgap $FeVO_4$. *Chem. Synth.* **2025**, *5*, 34. https://dx.doi.org/10.20517/cs.2024.159

Received: 4 Nov 2024 **First Decision:** 9 Dec 2024 **Revised:** 16 Jan 2025 **Accepted:** 17 Jan 2025 **Published:** 11 Mar 2025

Academic Editor: Jun Xu **Copy Editor:** Pei-Yun Wang **Production Editor:** Pei-Yun Wang

Abstract

The exploration of novel oxide photocatalysts with narrow bandgaps is highly desirable for efficient photocatalytic water splitting. However, this is rather challenging as reducing the bandgap generally leads to severe charge recombination in photocatalysts. To address these issues, the present work demonstrates, for the first time, the synthesis and application of triclinic $FeVO_4$ with an absorption edge of 575 nm for visible-light-driven photocatalytic water reduction and oxidation. Based on it, the Cr doping strategy is implemented on the $FeVO_4$ photocatalyst to further promote the charge separation and the photocatalytic water splitting performance, achieving an apparent quantum efficiency (AQE) of 0.26% at 420 nm (± 15 nm) for an O_2 evolution reaction. Detailed analysis shows that an impurity level below the conduction band minimum originating from the Cr 3*d* orbital is formed after Cr doping, facilitating the prolonged absorption edge and the enhanced charge separation. This work inaugurates the application field of the narrow bandgap particulate $FeVO_4$ photocatalyst in photocatalytic water splitting, and validates that charge separation can be promoted by Cr doping, both of which are promising to be further developed for efficient solar energy conversion.

Keywords: $FeVO_4$, Cr doping, narrow bandgap, photocatalytic water splitting, charge separation

INTRODUCTION

As an abundant and sustainable energy source, solar energy shows great potential in the application field of photocatalytic water splitting for green hydrogen production[1-3]. At present, most photocatalysts for photocatalytic water splitting are ultraviolet-light-responsive oxides, such as TiO_2, $SrTiO_3$, *etc.*[4,5]. However, in a photocatalytic process, the light absorption wavelength range of photocatalysts determines the maximum theoretical solar energy conversion efficiency[6,7]. Therefore, the development of narrow bandgap photocatalysts is the prerequisite to achieving an efficient solar water splitting process. To date, a series of visible-light-responsive oxides, nitrides, oxynitrides, sulfides, oxysulfides and selenides, including g-C_3N_4, $BiVO_4$, Ta_3N_5, $BaTaO_2N$, $Y_2Ti_2O_5S_2$, $(ZnSe)_x(CuGa_{2.5}Se_{4.25})_{1-x}$, *etc.*, have been demonstrated for photocatalytic water splitting[8-14]. Among those reported semiconductors, the oxides show the best thermal stability in the air and excellent photostability under illumination. However, currently, the number of demonstrated oxide photocatalysts with narrow bandgaps remains limited, especially for those capable of simultaneously achieving photocatalytic hydrogen evolution reaction (HER) and oxygen evolution reaction (OER). Another issue with narrow bandgap photocatalysts is that as the bandgap of the semiconductor decreases, severe charge recombination generally occurs, resulting in poor charge separation and low efficiency of photocatalytic HER and OER. Therefore, developing oxide photocatalysts with narrow bandgaps while possessing sufficient charge separation is still challenging for efficient solar-driven photocatalytic water splitting[15-18].

The iron vanadate ($FeVO_4$) is a narrow bandgap semiconductor with an absorption edge of 575 nm. Band structure analysis shows that its levels of the conduction band minimum (CBM) and the valance band maximum (VBM) are at -0.37 and 1.73 V [*vs.* normal hydrogen electrode (NHE)], respectively, which straddle the potentials of H^+/H_2 (0 V *vs.* NHE) and O_2/H_2O (1.23 V *vs.* NHE)[19-23]. It means that $FeVO_4$ meets the requirement for both photocatalytic HER and OER in thermodynamics. Up until now, various applications, such as photoelectrochemical (PEC) water splitting[24,25] and photocatalytic degradation of organic pollutants[26,27], have been investigated over $FeVO_4$ photo(electro)catalysts, demonstrating its excellent properties in optoelectronics. However, there is currently no report of particulate $FeVO_4$ photocatalysts for water splitting reaction. In addition, regarding the promotion of charge separation, series strategies, including doping of metal or nonmetal[28,29] and heterojunction construction[30,31], have been demonstrated to be effective for $FeVO_4$ photo(electro)catalysts. For example, it has been reported that the charge separation efficiency can be significantly enhanced by Cr doping over $FeVO_4$ photoanodes for PEC water splitting[32]. Therefore, it is anticipated that the promoted charge separation can also be achieved over $FeVO_4$ photocatalyst by using Cr as a dopant to further improve the water splitting activity.

In this work, we demonstrated that visible-light-driven water reduction and oxidation reactions could be realized over the triclinic $FeVO_4$ with an absorption edge of 575 nm loaded with proper cocatalysts. As far as we know, this is the first report of photocatalytic water splitting for the $FeVO_4$ photocatalysts. Based on this result, it was further identified that the promoted charge separation and enhanced photocatalytic water splitting performance could be achieved by implementing the Cr doping strategy to the $FeVO_4$ photocatalysts, in which an apparent quantum efficiency (AQE) of 0.26% at 420 nm (± 15 nm) was obtained for an OER. Detailed characterization results manifested that the Cr doping could produce an additional impurity level below the CBM of the $FeVO_4$ semiconductor, which could facilitate the prolonged absorption edge and inhibit charge recombination. Our results demonstrate the feasibility of $FeVO_4$ in achieving the photocatalytic water reduction and oxidation reactions, based on which the effectiveness of Cr doping in enhancing the charge separation is also illustrated.

EXPERIMENTAL

Synthesis of $FeVO_4$

The $FeVO_4 \cdot 1.1H_2O$ precursor was synthesized via a hydrothermal method, followed by calcination in air to obtain $FeVO_4$[19]. Typically, 10 mL of NH_4VO_3 (99%, Rhawn Chemical Reagent) aqueous solution (0.3 M) was added to 10 mL of $Fe(NO_3)_3 \cdot 9H_2O$ (99.5%, Macklin Chemical Reagent) aqueous solution (0.3 M). After continuously stirring for 0.5 h, the resulting suspension was transferred to a 100 mL Teflon-lined stainless-steel autoclave and heated at 453 K for 3 h. The $FeVO_4 \cdot 1.1H_2O$ precursor was collected by centrifugation, washed with deionized water several times and then dried in vacuum at 333 K for 6 h. Subsequently, the precursor was calcined in a muffle furnace at 823 K for 2 h to obtain $FeVO_4$.

Synthesis of $FeVO_4$:Cr

$FeVO_4$:Cr [the molar ratio of Cr/(Cr + Fe) is 0, 1.5%, 2.0%, 2.5%, 3.0% or 3.5%] was synthesized in a similar way to $FeVO_4$[33]. The Cr source [$Cr(NO_3)_3 \cdot 9H_2O$, 99%, Macklin Chemical Reagent] was added to the solution containing NH_4VO_3 and $Fe(NO_3)_3 \cdot 9H_2O$ for Cr doping. Then, the same hydrothermal treatment was implemented to obtain $FeVO_4$:Cr·$1.1H_2O$. After that, $FeVO_4$:Cr·$1.1H_2O$ was similarly calcined to obtain $FeVO_4$:Cr.

Preparation of $CoO_x/FeVO_4$ and $CoO_x/FeVO_4$:Cr by an impregnation method

Typically, 0.1 g of $FeVO_4$ or $FeVO_4$:Cr sample was dispersed in 1.0 mL of aqueous solution containing a calculated amount of [$Co(NO_3)_2 \cdot 6H_2O$ (99.9%, Aladdin Chemical Reagent)] and evaporated with a water bath. The collected powder was calcined at 573 K for 1 h.

Preparation of $CoO_x/FeVO_4$ by a photodeposition method

Typically, 0.1 g of $FeVO_4$ sample was dispersed in 100 mL of aqueous solution containing calculated amounts of $Co(NO_3)_2 \cdot 6H_2O$ and 20 mM of $NaIO_3$ (99.9%, Aladdin Chemical Reagent). The suspension was evacuated to completely remove the dissolved air and then exposed to visible light ($\lambda \geq 420$ nm) with continuous stirring for 2 h. The temperature of the reaction solution was maintained at 283 K by a chiller. After the reaction, the as-loaded powder was collected by filtration and dried naturally.

Preparation of $Pt/FeVO_4$ and $Pt/FeVO_4$:Cr by an impregnation-reduction method

Typically, 0.1 g of $FeVO_4$ or $FeVO_4$:Cr sample was dispersed in 1.0 mL of aqueous solution containing a calculated amount of H_2PtCl_6 (99.5%, Sinopharm Chemical) and totally evaporated with a water bath. The collected powder was calcined at 573 K for 2 h under Ar flow (100 mL/min). The resulting powder was added to 30 mL of $NaBH_4$ (98%, Energy Chemical Reagent) aqueous solution (0.2 mg/mL) to reduce the Pt^{4+} to Pt^0. After stirring for 10 min, the solution was filtered and dried in vacuum at 333 K for 6 h.

Photocatalytic H_2 evolution reaction

The photocatalytic HER was conducted in a Pyrex top-irradiation-type reactor vessel connected to a gas-closed-circulation system. Typically, 0.1 g of $Pt/FeVO_4$ or $Pt/FeVO_4$:Cr was added to 100 mL of aqueous solution containing ascorbic acid (10 mM, $C_6H_8O_6$, 99%, Aladdin Chemical Reagent) as a hole sacrificial reagent. The reactor was then connected to the system and thoroughly evacuated. The temperature of the reaction solution was maintained at about 283 K by a chiller. A 300 W Xenon lamp with a cut-off filter ($\lambda \geq 420$ nm) was used as a light source, and the produced H_2 gas was analyzed by online gas chromatography (Shimadzu, GC-2014, Ar as carrier gas).

Photocatalytic O_2 evolution reaction

The photocatalytic OER was carried out in the same gas-closed-circulation system with HER. Typically, 0.1 g of $CoO_x/FeVO_4$ or $CoO_x/FeVO_4$:Cr was added to 100 mL of aqueous solution containing $AgNO_3$

(50 mM) as an electron sacrificial reagent and 0.1 g of La_2O_3 (99.9%, Aladdin Chemical Reagent) was added to the solution to adjust the pH value to be about 8.5. The reactor was thoroughly evacuated by connecting to the system and was maintained at about 283 K. The photocatalytic reaction was conducted under a 300 W xenon lamp with a cut-off filter ($\lambda \geq 420$ nm), and the produced O_2 gas was analyzed by online gas chromatography.

Measurement of AQE

An AQE was measured using a 300 W Xe lamp with a band-pass filter (Beijing Perfectlight, UVCUT420) to illuminate a Pyrex top-irradiation-type reaction vessel, which was calculated by

$$\text{AQE}\ (\%) = \frac{AR}{I} \times 100$$

where A is a coefficient, which is 4 for oxygen evolution. R is the rate of oxygen evolution, and I is the number of photons measured at 420 nm. The total number of the incident photons was measured to be 7.27×10^{20} photons·h^{-1}.

Preparation of $FeVO_4$ and $FeVO_4$:Cr photoelectrodes

The photoelectrodes were prepared using an electrophoresis method. Firstly, 25 mg of $FeVO_4$ or $FeVO_4$:Cr (2.5%) was dispersed to 25 mL of acetone solution containing 10 mg of iodine. Two parallel pieces of fluorine-doped tin oxide (FTO) glass were immersed in the suspension. The positive and negative electrodes of the potentiostat were connected with the two FTO glass pieces, respectively, and a constant voltage of 30 V was applied for 5 min. The catalyst powder was uniformly deposited on the negative electrode. After the electrophoretic deposition, the photoelectrode was calcined at 573 K for 1 h to remove the charged species adsorbed on the surface of photocatalysts.

PEC measurements

The PEC measurements were conducted in a three-electrode system on an electrochemical workstation (CHI760E) by using a $FeVO_4$ or $FeVO_4$:Cr photoelectrode as the working electrode, a platinum sheet as the counter electrode, and an Ag/AgCl electrode (saturated KCl) as the reference electrode. Mott-Schottky test was performed in Na_2SO_4 solution (0.5 M) at a frequency of 500 or 1,000 Hz and a voltage from -1.0 to 1.0 V (*vs.* Ag/AgCl). Photocurrent density test was performed in Na_2SO_3 solution (0.5 M) and at a voltage of 0.5 V (*vs.* Ag/AgCl) by using a 300 W Xenon lamp with a cut-off filter ($\lambda \geq 420$ nm) as a light source. The measured potential at the Ag/AgCl electrode was converted to NHE using the Nernst equation.

Computational method

First-principles calculations were performed by the Vienna ab initio simulation package (VASP)[34,35]. The generalized gradient approximation (GGA) of Perdew-Burke-Ernzerhof (PBE) was employed to describe the exchange-correlation functional[36]. The cut-off energy for the plane wave basis was set to 400 eV and the Monkhorst-pack k-point mesh was set to 4 × 4 × 4. The structural relaxation was implemented until the forces were less than 0.01 eV/Å and the energy convergence of 10^{-5} eV was obtained.

To simulate the $FeVO_4$:Cr, an Fe atom in the $FeVO_4$ unit cell was replaced by the Cr atom. The Hubbard-type U correction for the strong-correlation d electrons of Fe, V and Cr was set to 3.5, 4.3 and 3.8 eV, respectively[37].

Characterization

The X-ray diffraction (XRD, Rigaku, Smart Lab) with Cu Kα radiation (λ = 1.5418 Å, 40 mA, 40 kV) was employed to investigate the crystalline structure of the prepared samples. The ultraviolet-visible diffuse

reflectance spectroscopy (UV-Vis DRS, Shimadzu, UV–2600i) was applied to gain insight into the optical property. A scanning electron microscope (SEM, JEOL, JSM-7800F) and a transmission electron microscope (TEM, JEOL, JEM-2800) were used to determine the morphology and elemental distribution of the catalysts. X-ray photoelectron spectroscopy (XPS, Thermo Scientific, ESCALAB 250Xi, the C 1*s* peak at 284.8 eV served as the internal standard for calibrating the binding energy) was performed to analyze the valence state of the catalyst surface. The chemical structure of the materials was characterized using microscopic confocal Raman spectroscopy (Raman, TEO, SR-500I-A) with a laser wavelength of 532 nm. The photoluminescence (PL) spectroscopy (Hitachi, F-7000) was used to determine the charge separation efficiency with an excitation wavelength of 310 nm. The Cr content was analyzed using an inductively coupled plasma optical emission spectrometer (ICP-OES, Thermo Fisher iCAP PRO).

RESULTS AND DISCUSSION

Characterization of $FeVO_4$ and photocatalytic performance

Typically, the $FeVO_4 \cdot 1.1H_2O$ precursor was prepared by the hydrothermal method, followed by the calcination treatment in the air to obtain $FeVO_4$ [Scheme 1][19]. As given in Supplementary Figure 1, the XRD pattern shows that the diffraction peaks of the $FeVO_4$ sample correspond to the standard pattern of the triclinic $FeVO_4$ (JCPDS#71-1592). A SEM image shows that the $FeVO_4 \cdot 1.1H_2O$ precursor possesses a smooth needle-like morphology with a length of about 3-4 μm and a diameter of about 100 nm [Supplementary Figure 2A]. After calcination at 823 K, the structure partially collapses due to dehydration, resulting in a rough surface [Supplementary Figure 2B]. The UV-Vis DRS of $FeVO_4$ exhibits a wide light absorption wavelength range, with an absorption edge of approximately 575 nm calculated from the Kubelka-Munk function [Figure 1A]. As displayed in Supplementary Figure 3, the positive slope of the Mott-Schottky plots implies that $FeVO_4$ is an n-type semiconductor, and the flat potential is estimated to be -0.37 V by the intersection point on the x-axis. For n-type semiconductors, the flat band potential can be approximated to the CBM[38]. Meanwhile, the bandgap is calculated to be 2.16 eV by Tauc plot [Supplementary Figure 4]. Therefore, the CBM and VBM of $FeVO_4$ are calculated to be -0.37 and 1.79 V, respectively [Figure 1B]. Based on this result, both the photocatalytic HER and OER over $FeVO_4$ are thermodynamically feasible.

Thus, the application of photocatalytic water splitting over $FeVO_4$ is investigated. For the OER, an oxidation cocatalyst of CoO_x was deposited on the $FeVO_4$ by the impregnation (Imp) method and photodeposition (PD) method before the evaluation (see the Experimental Section for details). As provided in Figure 1C, visible-light-driven photocatalytic OER can be achieved over the two photocatalysts, in which $CoO_x/FeVO_4$ prepared by the Imp method shows higher activity. For the HER, stable photocatalytic performance under visible light irradiation can also be realized over the $FeVO_4$ photocatalyst loaded with the reduction cocatalyst of Pt [Figure 1D]. Therefore, based on these results, it is concluded that both photocatalytic water oxidation and reduction reactions can be achieved over the $FeVO_4$ photocatalysts under visible light irradiation. To the best of our knowledge, this is the first report on the application of $FeVO_4$ for photocatalytic water splitting.

Doping strategy to promote the $FeVO_4$ photocatalysts

Although the as-developed $FeVO_4$ photocatalyst in this work can absorb visible light with wavelengths as long as 575 nm, the photocatalytic water splitting activity remains low, probably due to poor charge separation. To address this issue, element doping is investigated on the $FeVO_4$ photocatalyst water splitting[33]. Herein, the Cr-doped $FeVO_4 \cdot 1.1H_2O$ (denoted as $FeVO_4$:Cr·$1.1H_2O$) was prepared by adding a Cr source in the hydrothermal process, and then the calcination treatment in the air was implemented to obtain the $FeVO_4$:Cr sample (see the Experimental Section for details). In the following text, the molar ratio of Cr/(Cr + Fe) in $FeVO_4$:Cr is 2.5%, unless otherwise specified.

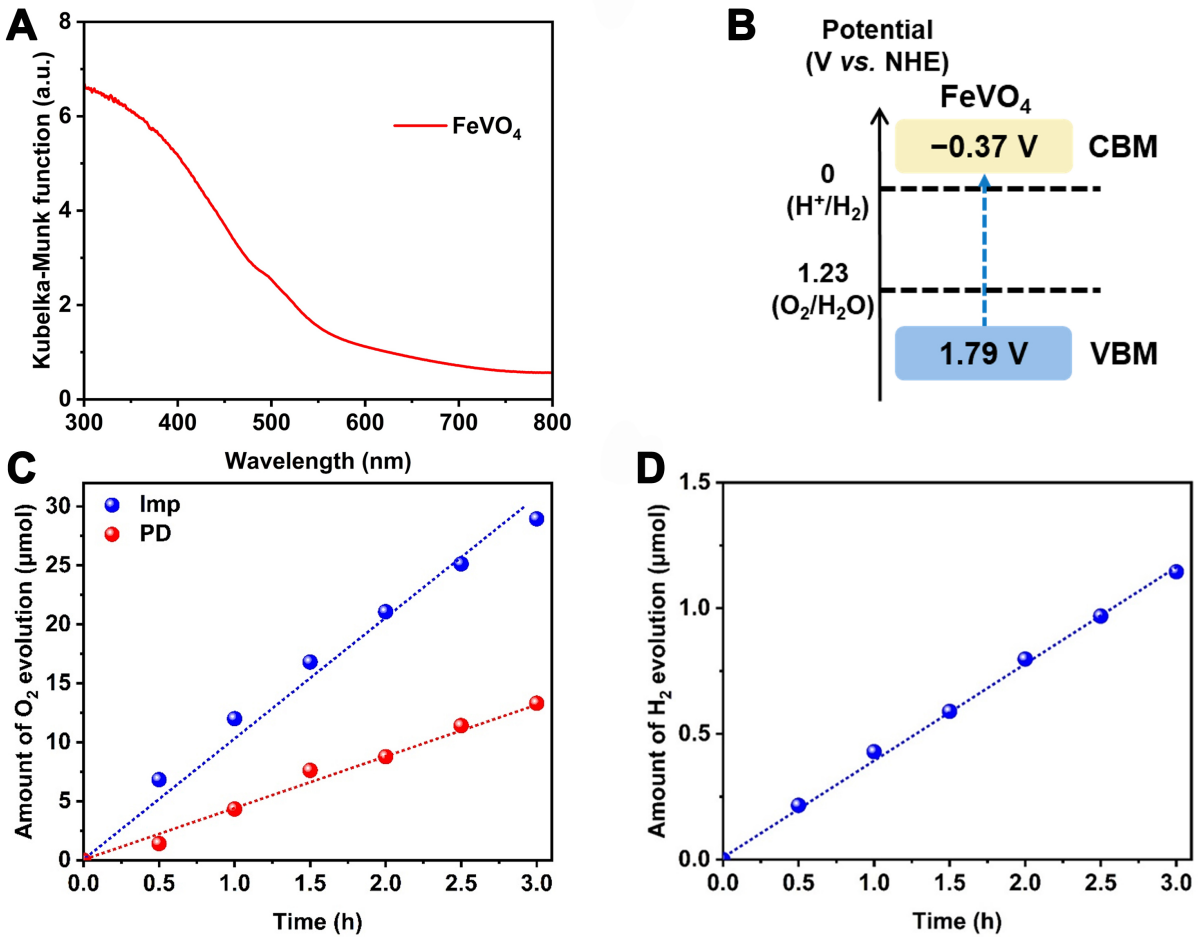

Figure 1. (A) UV-Vis DRS and (B) a schematic illustration of the band structure of $FeVO_4$; (C) Time courses of the OER over $FeVO_4$ photocatalysts loaded with CoO_x cocatalyst in different methods; (D) Time course of the HER over $FeVO_4$ photocatalyst loaded with Pt cocatalyst. Reaction conditions of (C): 0.1 g of photocatalyst (0.8 wt% Co is loaded); 100 mL of $AgNO_3$ aqueous solution (50 mM); 0.1 g of La_2O_3; 300 W Xe lamp with a cut-off filter ($\lambda \geq 420$ nm). Reaction conditions of (D): 0.1 g of photocatalyst (1.0 wt% Pt is loaded); 100 mL of ascorbic acid aqueous solution (10 mM); 300 W Xe lamp with a cut-off filter ($\lambda \geq 420$ nm). UV-Vis DRS: Ultraviolet-visible diffuse reflectance spectroscopy; OER: oxygen evolution reaction; HER: hydrogen evolution reaction.

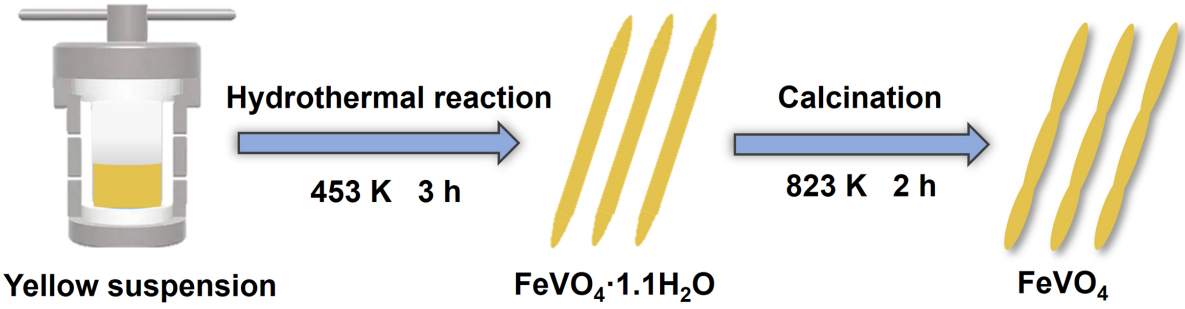

Scheme 1. Schematic of the preparation of $FeVO_4$ sample by the hydrothermal-calcination process.

Subsequently, the structure and distribution of elements in $FeVO_4$:Cr·$1.1H_2O$ and $FeVO_4$:Cr samples were further investigated to verify the success of the doping. Inductively coupled plasma optical emission

spectroscopy (ICP-OES) analysis indicates that Cr has been successfully introduced into $FeVO_4$ [Supplementary Table 1]. SEM images show that both $FeVO_4$:Cr·1.1H_2O and $FeVO_4$:Cr samples exhibit a similar morphology to that of the undoped case, suggesting the modification of Cr doping does not obviously influence the morphology [Supplementary Figure 5A and B]. Energy dispersive X-ray spectroscopy (EDS) mapping images confirm that the Cr dopant is uniformly distributed in the $FeVO_4$:Cr sample [Supplementary Figure 5C]. TEM images indicate that both $FeVO_4$ and $FeVO_4$:Cr samples exhibit porous structure due to the dehydration process, and the morphology is well maintained after Cr doping [Supplementary Figure 6A and B]. Furthermore, high crystallinity is also observed on both samples [Supplementary Figure 6C and D]. XRD patterns show that the crystal structure is maintained after the introduction of the Cr dopant [Supplementary Figure 7A]. However, a positive shift of the diffraction peaks is observed with increasing the proportion of the incorporated Cr element [Supplementary Figure 7B], demonstrating the substitution of Cr^{3+} ions for Fe^{3+} ions [the ionic radius of Cr^{3+} (62 pm) is smaller than that of Fe^{3+} (65 pm)][39]. Further information of the Rietveld refinement for those XRD patterns indicates that the substitution of Cr^{3+} ions for Fe^{3+} ions leads to the contraction of the a-axis, b-axis and c-axis of the $FeVO_4$ unit cell, along with a decrease in the β angle [Supplementary Figure 8 and Supplementary Table 2]. The Raman spectra also show similar results based on

$$\nu\ (cm^{-1}) = 21349e^{-1.976R(Å)}$$

where ν is the Raman vibration frequency and R is the estimated bond length[40,41]. In other words, the Raman vibration frequency is inversely proportional to the bond length. The peaks at 720 and 822 cm^{-1} ascribing to bridging V-O···Fe bond stretching mode shift to higher wavenumbers after Cr doping, indicating that the length becomes shorter [Supplementary Figure 9]. This is consistent with the results of the data for the lattice parameters. UV-Vis DRS shows that the Cr doping can induce a slight redshift of the absorption edge from 575 to 585 nm for the $FeVO_4$-based samples [Supplementary Figure 10]. These results indicate that Cr was successfully doped into $FeVO_4$, widening the absorption edge.

Apart from the effect of Cr doping on the structure and morphology, its influence on the chemical state of the elements after Cr doping was also examined. As shown in Supplementary Figure 11A, the high-resolution Cr 2*p* XPS of $FeVO_4$ and $FeVO_4$:Cr samples reveal two characteristic peaks of $FeVO_4$:Cr at 576.5 and 587.2 eV corresponding to Cr^{3+} $2p_{3/2}$ and Cr^{3+} $2p_{1/2}$, respectively, indicating that the valence state of Cr is consistent with Fe in $FeVO_4$[42]. In the meantime, two peaks at the same binding energies of 711.2 and 725.6 eV are observed on $FeVO_4$ and $FeVO_4$:Cr samples, which correspond to Fe^{3+} $2p_{3/2}$ and Fe^{3+} $2p_{1/2}$, respectively [Supplementary Figure 11B][43]. In addition, in the high-resolution V 2*p* and O 1*s* XPS of $FeVO_4$ and $FeVO_4$:Cr samples, the characteristic peaks at 517.1, 524.6 and 530.3 eV correspond to V^{5+} $2p_{1/2}$, V^{5+} $2p_{3/2}$, and O^{2-} 1*s*, respectively [Supplementary Figure 11C and D][44,45]. Therefore, the incorporation of Cr does not change the valence states of Fe, V and O. Therefore, it can be concluded that there is no obvious effect of Cr doping on the chemical states of $FeVO_4$ photocatalysts.

As Cr was successfully doped into $FeVO_4$, the photocatalytic activity of $FeVO_4$:Cr was further investigated. For the OER, under the optimized Cr doping proportion [Figure 2A] and the loading condition of CoO_x cocatalyst [Supplementary Figure 12], the maximum O_2 evolution rate of CoO_x/$FeVO_4$:Cr [the molar ratio of Cr/(Cr + Fe) is 2.5%] is 17.6 μmol/h, higher than that of CoO_x/$FeVO_4$ (12.1 μmol/h). The corresponding AQE for OER over the CoO_x/$FeVO_4$:Cr photocatalyst is 0.26% at 420 nm (± 15 nm). In addition, the Cr doping strategy for the promoted photocatalytic activity has also been similarly confirmed in another case of HER. As can be seen from Figure 2B, as the molar ratio of Cr/(Cr + Fe) increases from 0% to 4%, the H_2 evolution rate follows a volcano-shaped tendency with a maximum value at the ratio of 3%, about three

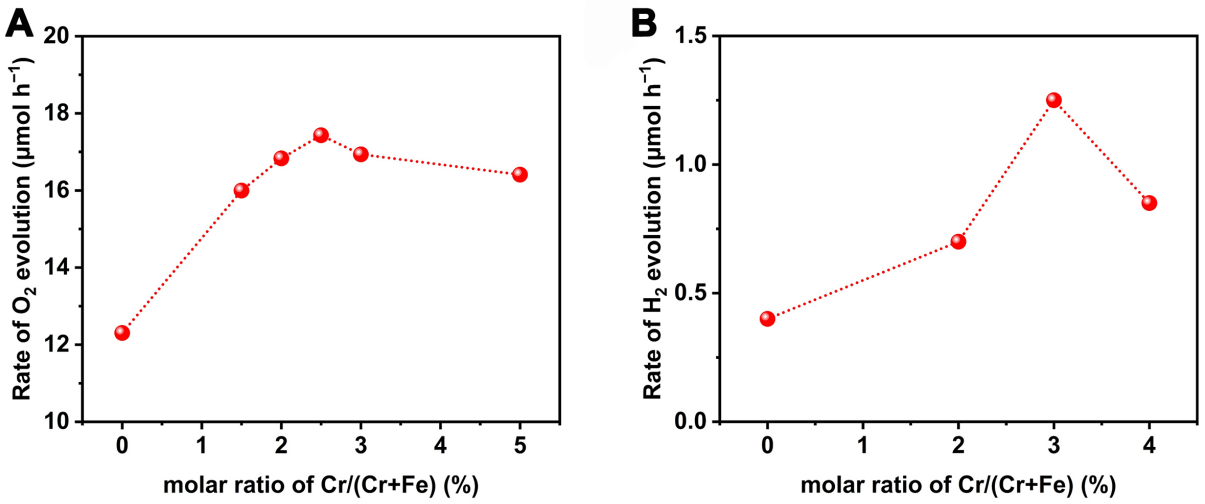

Figure 2. Effect of different molar ratios of Cr/(Cr + Fe) on (A) the photocatalytic O_2 evolution rate or (B) the photocatalytic H_2 evolution rate over $FeVO_4$. Reaction conditions for (A): 0.1 g of photocatalyst (0.8 wt% Co is loaded); 100 mL of $AgNO_3$ aqueous solution (50 mM); 0.1 g of La_2O_3; 300 W Xe lamp with a cut-off filter ($\lambda \geq 420$ nm). Reaction condition for (B): 0.1 g of photocatalyst (1.0 wt% Pt is loaded); 100 mL of ascorbic acid aqueous solution (10 mM); 300 W Xe lamp with a cut-off filter ($\lambda \geq 420$ nm).

times as high as that of the undoped photocatalyst. Herein, the optimized loading proportion of Pt is 1.0 wt% [Supplementary Figure 13]. In addition, the recycling test and XRD results indicate that $FeVO_4$:Cr (3.0%) also possesses outstanding stability [Supplementary Figure 14].

The origin of Cr doping for the enhanced photocatalytic performance

To determine the influence of Cr dopants on the photogenerated charge separation, firstly, PEC characterization is applied to compare their photocurrent densities in Na_2SO_3 solution under visible light irradiation [Figure 3A]. In this circumstance, the effect of charge injection efficiency can be excluded due to the existence of the hole scavenger. Considering both samples of $FeVO_4$ and $FeVO_4$:Cr have similar absorption edges, the difference in the photocurrent density is primarily attributed to the distinct charge separation. It can be obviously observed that $FeVO_4$:Cr photoanode exhibits higher photocurrent density than $FeVO_4$ photoanode, indicating the former possesses higher charge separation efficiency. Such a conclusion can be further identified by the PL spectra. As shown in Figure 3B, an emission peak at approximately 625 nm is detected for both samples, in which the $FeVO_4$:Cr sample exhibits a much lower peak intensity, suggesting that charge recombination can be effectively inhibited by the Cr doping treatment.

As is known, photocatalytic efficiency is determined by three basic processes: light absorption, charge separation, and surface catalytic conversion. Herein, two factors, other than charge separation, are further investigated to determine their contribution to the enhancement of photocatalytic activity. The absorption edge can be slightly extended by the Cr doping over the $FeVO_4$ semiconductor, which can enhance the light-harvesting efficiency to a certain degree. Regarding surface catalytic conversion, the loaded CoO_x cocatalyst is mainly studied. It is confirmed the binding energies at 781.4 eV ($2p_{3/2}$) and 797.3 eV ($2p_{1/2}$) in the Co 2*p* XPS data of both $CoO_x/FeVO_4$ and $CoO_x/FeVO_4$:Cr samples are the same [Supplementary Figure 15], indicating that Cr doping does not alter the chemical state of the CoO_x cocatalyst[46]. Additionally, similar particle size and morphology of the deposited CoO_x are identified for $CoO_x/FeVO_4$ and $CoO_x/FeVO_4$:Cr samples [Supplementary Figure 16]. Based on these analyses, the distinction in the surface catalytic conversion between the two samples can be excluded. In conclusion, the improved photocatalytic

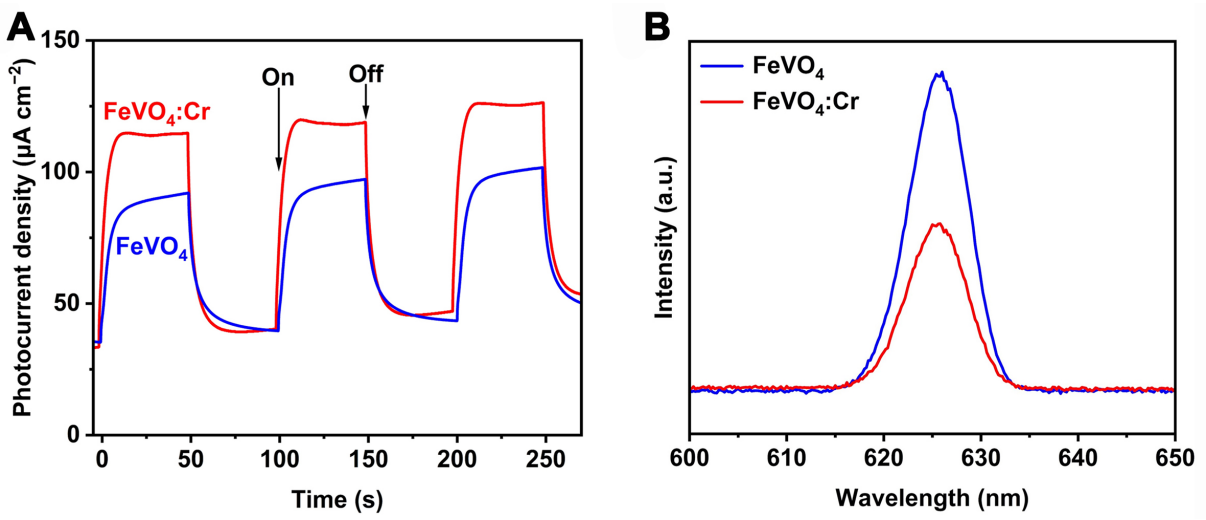

Figure 3. (A) The photocurrent densities of $FeVO_4$ and $FeVO_4$:Cr photoanodes at 1.0 V *vs.* NHE in Na_2SO_3 aqueous solution under visible light (≥ 420 nm); (B) PL spectra of $FeVO_4$ and $FeVO_4$:Cr samples. NHE: Normal hydrogen electrode; PL: photoluminescence.

water splitting performance is primarily attributed to the extended light absorption and enhanced charge separation due to Cr doping.

To reveal the origin of the extension in the light absorption edge and the enhancement of the charge separation, the density of states (DOS) was calculated. The crystal structure models of $FeVO_4$ and $FeVO_4$:Cr are given in Figure 4A and B, in which the latter case is constructed by replacing an Fe atom with a Cr atom. As shown in Figure 4C, the CBM and VBM of $FeVO_4$ are mainly contributed by Fe 3*d* and O 2*p* orbitals, respectively. After Cr doping, an impurity level originating from the Cr 3*d* orbital is observed below the CBM [Figure 4D]. This impurity level induces a slight downshift of the CBM, leading to a decrease in the bandgap and facilitating the charge separation [Figure 4E].

CONCLUSIONS

In summary, it was demonstrated, for the first time, that the $FeVO_4$ photocatalyst with an absorption edge of 575 nm could drive both photocatalytic water reduction and oxidation under visible light irradiation. After Cr doping, the corresponding photocatalytic water splitting activities could be efficiently promoted. Detailed analysis shows that the strategy of Cr doping can prolong the absorption edge and enhance the charge separation of the $FeVO_4$ photocatalyst, contributing to improved photocatalytic water splitting performance. This work inaugurates a new application field of photocatalytic water splitting for $FeVO_4$ semiconductors with a narrow bandgap, and identifies that Cr doping is an effective strategy to further promote the $FeVO_4$ photocatalysts, both of which are expected to be extended to other photocatalytic reaction systems for efficient solar energy conversion.

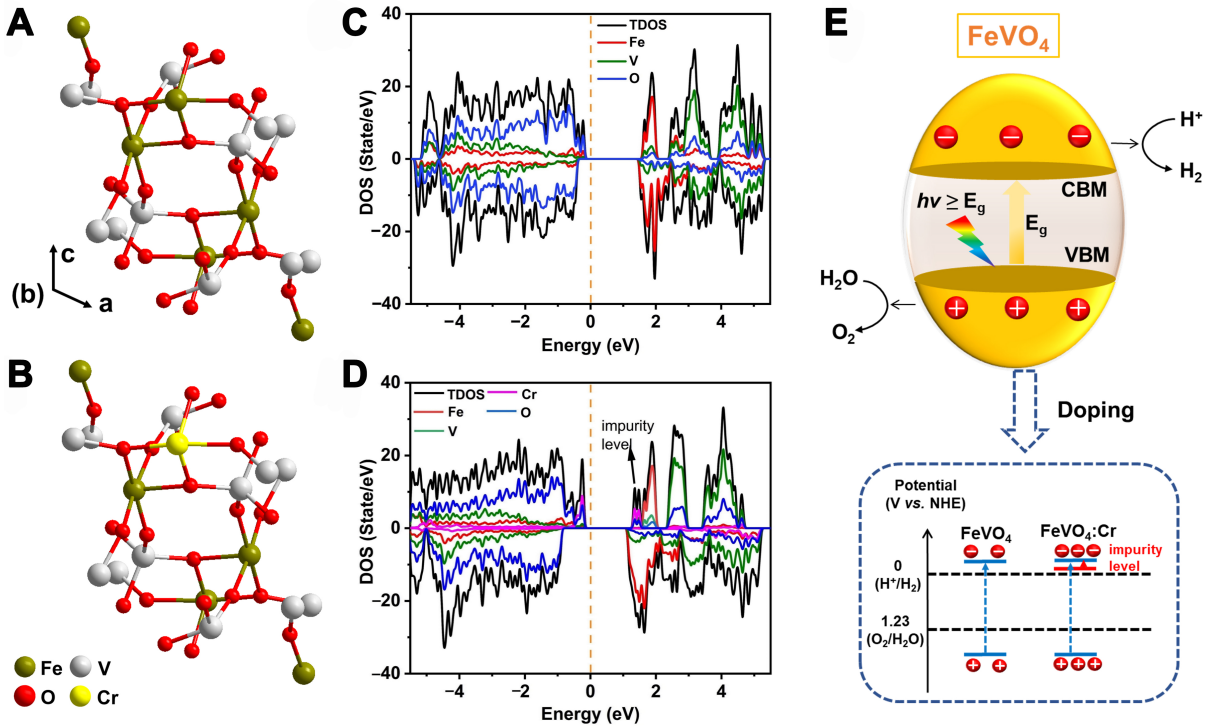

Figure 4. Optimized atomistic models of (A) $FeVO_4$ and (B) $FeVO_4$:Cr samples and the DOS of (C) $FeVO_4$ and (D) $FeVO_4$:Cr samples; (E) Schematic diagram of $FeVO_4$ with or without Cr doping for photocatalytic water splitting. DOS: Density of states.

DECLARATIONS

Authors' contributions

Conception and design of the study: Chen, S.; Zhang, F.
Data collection and analysis: Wang, S.; Liu, C.
Sample preparation: Li, C.; Wang, N.; Li, C. Y.; Yuan, Z.
Paper writing and reviewing: Wang, S.; Liu, C.; Chen, S.; Zhang, F.

Availability of data and materials

Some results of supporting the study are presented in the Supplementary Materials. Other raw data that support the findings of this study are available from the corresponding author upon reasonable request.

Financial support and sponsorship

We are grateful for the financial support from the National Natural Science Foundation of China (22272082, 21925206), the Fundamental Research Funds for the Central Universities, Nankai University (63213098), and the Foundation from Hebei Provincial Department of Science and Technology (226Z4307G).

Conflicts of interest

All authors declared that there are no conflicts of interest.

Ethical approval and consent to participate

Not applicable.

Consent for publication

Not applicable.

REFERENCES

1. Nishioka, S.; Osterloh, F. E.; Wang, X.; Mallouk, T. E.; Maeda, K. Photocatalytic water splitting. *Nat. Rev. Methods. Primers.* **2023**, *3*, 42. DOI
2. Sun, K.; Qian, Y.; Jiang, H. L. Metal-organic frameworks for photocatalytic water splitting and CO_2 reduction. *Angew. Chem. Int. Ed. Engl.* **2023**, *62*, e202217565. DOI PubMed
3. Lin, L.; Yu, Z.; Wang, X. Crystalline carbon nitride semiconductors for photocatalytic water splitting. *Angew. Chem. Int. Ed. Engl.* **2019**, *58*, 6164-75. DOI
4. Bai, Y.; Zhou, Y.; Zhang, J.; et al. Homophase junction for promoting spatial charge separation in photocatalytic water splitting. *ACS. Catal.* **2019**, *9*, 3242-52. DOI
5. Takata, T.; Jiang, J.; Sakata, Y.; et al. Photocatalytic water splitting with a quantum efficiency of almost unity. *Nature* **2020**, *581*, 411-4. DOI
6. Zhang, Y.; Zhao, J.; Wang, H.; et al. Single-atom Cu anchored catalysts for photocatalytic renewable H_2 production with a quantum efficiency of 56%. *Nat. Commun.* **2022**, *13*, 58. DOI PubMed PMC
7. Li, Y.; Peng, Y. K.; Hu, L.; et al. Photocatalytic water splitting by N-TiO_2 on MgO (111) with exceptional quantum efficiencies at elevated temperatures. *Nat. Commun.* **2019**, *10*, 4421. DOI PubMed PMC
8. Lin, L.; Lin, Z.; Zhang, J.; et al. Molecular-level insights on the reactive facet of carbon nitride single crystals photocatalysing overall water splitting. *Nat. Catal.* **2020**, *3*, 649-55. DOI
9. Wang, Y.; Huang, W.; Guo, S.; et al. Sulfur-deficient $ZnIn_2S_4$/oxygen-deficient WO_3 hybrids with carbon layer bridges as a novel photothermal/photocatalytic integrated system for Z-scheme overall water splitting. *Adv. Energy. Mater.* **2021**, *11*, 2102452. DOI
10. Dong, C.; Lu, S.; Yao, S.; et al. Colloidal synthesis of ultrathin monoclinic $BiVO_4$ nanosheets for Z-scheme overall water splitting under visible light. *ACS. Catal.* **2018**, *8*, 8649-58. DOI
11. Qi, Y.; Zhang, B.; Zhang, G.; et al. Efficient overall water splitting of a suspended photocatalyst boosted by metal-support interaction. *Joule* **2024**, *8*, 193-203. DOI
12. Chen, S.; Ma, G.; Wang, Q.; et al. Metal selenide photocatalysts for visible-light-driven *Z*-scheme pure water splitting. *J. Mater. Chem. A.* **2019**, *7*, 7415-22. DOI
13. He, Y.; Thorne, J.; Wu, C.; et al. What limits the performance of Ta_3N_5 for solar water splitting? *Chem* **2016**, *1*, 640-55. DOI
14. Zhang, J.; Liu, K.; Zhang, B.; et al. Anisotropic charge migration on perovskite oxysulfide for boosting photocatalytic overall water splitting. *J. Am. Chem. Soc.* **2024**, *146*, 4068-77. DOI
15. Jiang, L.; Yang, J.; Zhou, S.; et al. Strategies to extend near-infrared light harvest of polymer carbon nitride photocatalysts. *Coord. Chem. Rev.* **2021**, *439*, 213947. DOI
16. Fujito, H.; Kunioku, H.; Kato, D.; et al. Layered perovskite oxychloride Bi_4NbO_8Cl: a stable visible light responsive photocatalyst for water splitting. *J. Am. Chem. Soc.* **2016**, *138*, 2082-5. DOI
17. Lian, Z.; Sakamoto, M.; Kobayashi, Y.; et al. Anomalous photoinduced hole transport in type I core/mesoporous-shell nanocrystals for efficient photocatalytic H_2 evolution. *ACS. Nano.* **2019**, *13*, 8356-63. DOI
18. Wang, R.; He, H.; Shi, L.; et al. Unleashing photocarrier transport in mesoporous single-crystalline $LaTiO_2N$ for high-efficiency photocatalytic water splitting. *Adv. Energy. Mater.* **2024**, *14*, 2302996. DOI
19. Ma, H.; Yang, X.; Tao, Z.; Liang, J.; Chen, J. Controllable synthesis and characterization of porous $FeVO_4$ nanorods and nanoparticles. *CrystEngComm* **2011**, *13*, 897-901. DOI
20. Zhao, Y.; Yao, K.; Cai, Q.; et al. Hydrothermal route to metastable phase $FeVO_4$ ultrathin nanosheets with exposed {010} facets: synthesis, photocatalysis and gas-sensing. *CrystEngComm* **2014**, *16*, 270-6. DOI
21. Sajid, M. M.; Zhai, H.; Shad, N. A.; et al. Photocatalytic performance of ferric vanadate ($FeVO_4$) nanoparticles synthesized by hydrothermal method. *Mater. Sci. Semicond. Process.* **2021**, *129*, 105785. DOI
22. Zhang, M.; Fang, Y.; Tay, Y. F.; et al. Nanostructured iron vanadate photoanodes with enhanced visible absorption and charge separation. *ACS. Appl. Energy. Mater.* **2022**, *5*, 3409-16. DOI
23. Chen, H.; Zeng, J.; Chen, M.; et al. Improved visible light photocatalytic activity of mesoporous $FeVO_4$ nanorods synthesized using a reactable ionic liquid. *Chin. J. Catal.* **2019**, *40*, 744-54. DOI
24. Zhang, M.; Ma, Y.; Friedrich, D.; van de Krol, R.; Wong, L. H.; Abdi, F. F. Elucidation of the opto-electronic and photoelectrochemical properties of $FeVO_4$ photoanodes for solar water oxidation. *J. Mater. Chem. A.* **2018**, *6*, 548-55. DOI
25. Wang, W.; Zhang, Y.; Wang, L.; Bi, Y. Facile synthesis of Fe^{3+}/Fe^{2+} self-doped nanoporous $FeVO_4$ photoanodes for efficient solar water splitting. *J. Mater. Chem. A.* **2017**, *5*, 2478-82. DOI
26. Alsulami, Q. A.; Rajeh, A.; Mannaa, M. A.; Albukhari, S. M.; Baamer, D. F. Preparation of highly efficient sunlight driven

photodegradation of some organic pollutants and H_2 evolution over rGO/$FeVO_4$ nanocomposites. *Int. J. Hydrog. Energy.* **2021**, *46*, 27349-63. DOI

27. Luangwanta, T.; Chachvalvutikul, A.; Kaowphong, S. Facile synthesis and enhanced photocatalytic activity of a novel $FeVO_4$/$Bi_4O_5Br_2$ heterojunction photocatalyst through step-scheme charge transfer mechanism. *Colloid. Surface. A.* **2021**, *627*, 127217. DOI
28. Naqvi, S. Q.; Jennings, J. R.; Raza, S. A.; Soon, Y. W.; Liu, Y. Hole collection and surface kinetics in Mo-doped $FeVO_4$ photoanodes during photoelectrochemical water oxidation. *ACS. Appl. Energy. Mater.* **2023**, *6*, 211-21. DOI
29. Zeng, Q.; Fu, X.; Chang, S.; et al. Ordered Ti-doped $FeVO_4$ nanoblock photoanode with improved charge properties for efficient solar water splitting. *J. Colloid. Interface. Sci.* **2021**, *604*, 562-7. DOI
30. Zhang, M.; Pham, H. K.; Fang, Y.; Tay, Y. F.; Abdi, F. F.; Wong, L. H. The synergistic effect of cation mixing in mesoporous $Bi_xFe_{1-x}VO_4$ heterojunction photoanodes for solar water splitting. *J. Mater. Chem. A.* **2019**, *7*, 14816-24. DOI
31. Balu, S.; Chen, Y. L.; Chen, S. W.; Yang, T. C. K. Rational synthesis of $Bi_xFe_{1-x}VO_4$ heterostructures impregnated sulfur-doped g-C_3N_4: a visible-light-driven type-II heterojunction photo(electro)catalyst for efficient photodegradation of roxarsone and photoelectrochemical OER reactions. *Appl. Catal. B. Environ.* **2022**, *304*, 120852. DOI
32. Nguyen, T. H.; Zhang, M.; Septina, W.; et al. High throughput discovery of effective metal doping in $FeVO_4$ for photoelectrochemical water splitting. *Solar. RRL.* **2020**, *4*, 2000437. DOI
33. Dutta, D. P.; Ramakrishnan, M.; Roy, M.; Kumar, A. Effect of transition metal doping on the photocatalytic properties of $FeVO_4$ nanoparticles. *J. Photochem. Photobiol. A.* **2017**, *335*, 102-11. DOI
34. Kresse, G.; Furthmüller, J. Efficiency of ab-initio total energy calculations for metals and semiconductors using a plane-wave basis set. *Comput. Mater. Sci.* **1996**, *6*, 15-50. DOI
35. Kresse, G.; Joubert, D. From ultrasoft pseudopotentials to the projector augmented-wave method. *Phys. Rev. B.* **1999**, *59*, 1758. DOI
36. Perdew, J. P.; Burke, K.; Ernzerhof, M. Generalized gradient approximation made simple. *Phys. Rev. Lett.* **1996**, *77*, 3865-8. DOI PubMed
37. Anisimov, V. I.; Zaanen, J.; Andersen, O. K. Band theory and Mott insulators: Hubbard *U* instead of Stoner *I*. *Phys. Rev. B.* **1991**, *44*, 943. DOI
38. Zhen, C.; Chen, X.; Chen, R.; et al. Liquid metal-embraced photoactive films for artificial photosynthesis. *Nat. Commun.* **2024**, *15*, 1672. DOI PubMed PMC
39. Shannon, R. D. Revised effective ionic radii and systematic studies of interatomic distances in halides and chalcogenides. *Acta. Cryst. A.* **1976**, *32*, 751-67. DOI
40. Thalluri, S. M.; Martinez, S. C.; Hussain, M.; et al. Evaluation of the parameters affecting the visible-light-induced photocatalytic activity of monoclinic $BiVO_4$ for water oxidation. *Ind. Eng. Chem. Res.* **2013**, *52*, 17414-8. DOI
41. Brown, I. D.; Wu, K. K. Empirical parameters for calculating cation–oxygen bond valences. *Acta. Crystallogr. B. Struct. Sci.* **1976**, *32*, 1957-9. DOI
42. Wu, Y.; Tao, X.; Qing, Y.; et al. Cr-doped FeNi-P nanoparticles encapsulated into N-doped carbon nanotube as a robust bifunctional catalyst for efficient overall water splitting. *Adv. Mater.* **2019**, *31*, 1900178. DOI
43. Marshall-Roth, T.; Libretto, N. J.; Wrobel, A. T.; et al. A pyridinic Fe-N_4 macrocycle models the active sites in Fe/N-doped carbon electrocatalysts. *Nat. Commun.* **2020**, *11*, 5283. DOI PubMed PMC
44. Pei, H.; Peng, L.; Jiang, Z.; Zhang, Y.; Li, R.; Peng, T. Gradient-tuned VO_4 vacancies in $BiVO_4$ photoanode for boosting bulk hole transport and oxygen evolution reaction performance. *Adv. Funct. Mater.* **2024**, *34*, 2401122. DOI
45. Wang, S.; He, T.; Chen, P.; et al. In situ formation of oxygen vacancies achieving near-complete charge separation in planar $BiVO_4$ photoanodes. *Adv. Mater.* **2020**, *32*, 2001385. DOI
46. Liu, M.; Zhang, G.; Liang, X.; et al. Rh/Cr_2O_3 and CoO_x cocatalysts for efficient photocatalytic water splitting by poly (triazine imide) crystals. *Angew. Chem. Int. Ed. Engl.* **2023**, *62*, e202304694. DOI

Shuo Wang

Shuo Wang received his master's degree from Nankai University in 2022. He is currently a Ph.D. student at Nankai University under the supervision of Prof. Shanshan Chen. His research interest focuses on surface-modified vanadates for photocatalytic water oxidation.

Chunjiang Liu

Chunjiang Liu received his master's degree from Nankai University in 2024 under the supervision of Prof. Shanshan Chen. His research interest centers on the development of oxide materials for photocatalytic water splitting.

Can Li

Can Li received her master's degree in 2021. She is currently a Ph.D. student at Nankai University under the supervision of Prof. Shanshan Chen. Her research explores the development of innovative electrocatalytic materials for water splitting.

Ningning Wang

Ningning Wang received her master's degree from Central China Normal University. She is currently a Ph.D. student at Nankai University under the supervision of Prof. Shanshan Chen. Her research interest focuses on the surface modification of tantalum-based (oxy)nitrides for photocatalytic water splitting.

Chen-Yang Li

Chen-Yang Li received his master's degree from Northwest University in 2021. He is currently a Ph.D. student at Nankai University under the supervision of Prof. Shanshan Chen. His research investigates the synthesis of particulate metal sulfides for photocatalytic Z-scheme overall water splitting.

Zhongxu Yuan

Zhongxu Yuan began his master's degree at Nankai University in 2022 under the supervision of Prof. Shanshan Chen. His research delves into the flux-assisted nitridation preparation of metal (oxy)nitrides for photocatalytic water splitting.

Shanshan Chen

Prof. Shanshan Chen received his Ph.D. in 2015 from DICP, Chinese Academy of Sciences. He then started his postdoctoral research at the University of Tokyo and Shinshu University, respectively, under the guidance of Prof. Kazunari Domen. In 2021, he joined Nankai University as a professor. His current research interests include the development of novel narrow bandgap semiconductors and their assembled artificial photosynthesis systems for efficient solar fuel production.

Fuxiang Zhang

Prof. Fuxiang Zhang is currently a full professor of physical chemistry at DICP and a fellow of the Royal Society of Chemistry (FRSC). He obtained his BSc in 1999 and Ph.D. in 2004 from Nankai University, where he subsequently began his academic career. From 2007 to 2011, he conducted postdoctoral research at the University of Pierre & Marie Curie in France, followed by further research at the University of Tokyo. His current research interests focus on the development of novel photocatalytic materials and the construction of photocatalytic and electrocatalytic systems for solar-to-chemical energy conversion.